

Document Version

Final published version

Citation (APA)

Sarkar, E., Cardoso, F. A., & Costa, T. L. (2025). MEMS-Based Design for Single-Pulsed High-Pressure Ultrasound System via Acoustic Amplification Through Acoustic Energy Storage and Release: Theory and Simulation. In *2025 IEEE International Ultrasonics Symposium, IUS 2025* (IEEE International Ultrasonics Symposium, IUS). IEEE. <https://doi.org/10.1109/IUS62464.2025.11201696>

Important note

To cite this publication, please use the final published version (if applicable). Please check the document version above.

Copyright

In case the licence states "Dutch Copyright Act (Article 25fa)", this publication was made available Green Open Access via the TU Delft Institutional Repository pursuant to Dutch Copyright Act (Article 25fa, the Taverne amendment). This provision does not affect copyright ownership. Unless copyright is transferred by contract or statute, it remains with the copyright holder.

Sharing and reuse

Other than for strictly personal use, it is not permitted to download, forward or distribute the text or part of it, without the consent of the author(s) and/or copyright holder(s), unless the work is under an open content license such as Creative Commons.

Takedown policy

Please contact us and provide details if you believe this document breaches copyrights. We will remove access to the work immediately and investigate your claim.

**Green Open Access added to [TU Delft Institutional Repository](#)
as part of the Taverne amendment.**

More information about this copyright law amendment
can be found at <https://www.openaccess.nl>.

Otherwise as indicated in the copyright section:
the publisher is the copyright holder of this work and the
author uses the Dutch legislation to make this work public.

MEMS-Based Design for Single-Pulsed High-Pressure Ultrasound System via Acoustic Amplification Through Acoustic Energy Storage and Release: Theory and Simulation

Eshani Sarkar

Department of Microelectronics
Delft University of Technology
Delft, The Netherlands
E.Sarkar@tudelft.nl

Filipe Arroyo Cardoso

Department of Microelectronics
Delft University of Technology
Delft, The Netherlands
F.ArroyoCardoso@tudelft.nl

Tiago L. Costa

Department of Microelectronics
Delft University of Technology
Delft, The Netherlands
T.M.L.daCosta@tudelft.nl

Abstract— Emerging biomedical ultrasound applications such as pulsed neurostimulation and shear-wave imaging demand single-pulse focused ultrasound waves with MPa-range acoustic pressures. Achieving high pressures typically involves driving transducers with high voltages, necessitating bulky power amplifiers. Recently, phased arrays have emerged to miniaturize these focused transducers. However, they often exhibit poor power efficiency and heat dissipation. To address this, we explore acoustic amplification through acoustic energy storage and release, where, with minimal voltage, high-amplitude ultrasound waves are produced. Prior work has shown the principle using bulky apparatus with limited applicability. In this work, we explore the theory and perform finite element modeling (FEM) to investigate this mechanism with miniaturized and micro-electro-mechanical systems (MEMS)-compatible materials and geometries.

Keywords – single pulse, acoustic amplification, acoustic resonant cavity, high acoustic pressure, ultrasound neuromodulation, ultrasound imaging

I. INTRODUCTION

Advances in biomedical ultrasound applications like transcranial pulse neurostimulation (TPS) [1] and shear wave imaging [2] demand high-pressure single-pulse focused ultrasound waves. Particularly, TPS often requires acoustic pressures in the MPa range and ultra-short single-pulses, which are generated by bulky commercially available focused ultrasound transducers that are driven with large voltages and bulky power amplifiers. To miniaturize these devices, miniaturized 2D phased arrays have emerged, with ultrasound transducers directly integrated on top of complementary metal-oxide-semiconductor (CMOS) circuits. This integration lowers parasitic capacitance and improves power efficiency. However, these systems still face trade-offs. In [3], capacitive micromachined ultrasound transducers (CMUTs) integrated on CMOS, were driven at 60 V, which resulted in extreme heating up to 141 °C peak temperature. In [4], integrated bulk piezoelectric transducers (PZT) on top of CMOS circuits were proposed; however, the device was limited to a power supply of 5 V, which limited the generated acoustic peak pressure to 100 kPa. As a result, current systems fail to deliver the ideal combination of high-acoustic output pressure and low driving voltage. This becomes more important when wearable, battery-powered

This work was funded by the European Union's Horizon Europe EIC-PATHFINDER programme under grant agreement No 101070931

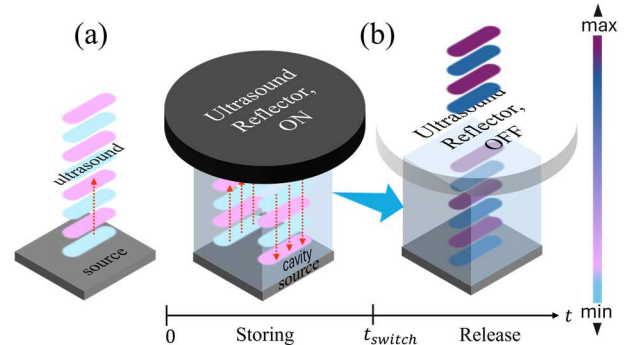


Fig. 1. Concept illustration of acoustic amplification through acoustic energy storage and release; (a) An acoustic source emitting continuous planar sinusoidal waves; (b) Acoustic energy emitted from the source is getting stored in an acoustic resonant cavity with time in presence of ultrasound reflector and releases with high-amplitude when the reflector is taken off at t_{switch} . Figures not drawn to scale.

ultrasound devices are considered, where generating tens of volts from small batteries is challenging [5], [6], [7]. To address this, we explore acoustic amplification through acoustic energy storage and release, aiming to enable miniaturized, energy-efficient generation of high-pressure single pulses. Prior work in industrial applications has demonstrated a similar concept for amplifying airborne ultrasound pulses [8]. The system used an acoustic cavity, to which was attached a rotating shutter with a small-aperture opening, facilitating the storage and release of acoustic energy. Although results showed 2.5 times pressure amplification, the bulky design made it unsuitable for miniaturized focused ultrasound devices.

This work introduces the theoretical and modeling framework for a miniaturized MEMS-compatible single-pulse ultrasound system that explores the above-mentioned principle by accumulating acoustic energy in a resonant cavity and releasing it in ultra-short, high-intensity pulses by means of a MEMS shutter.

This paper is organized as follows: Section II introduces the theoretical framework of acoustic amplification. Section III describes its finite element modeling approach, simulation results, and discussion. Section IV proposes the MEMS-based electrostatic actuator design as the MEMS shutter. Finally, Section V concludes the paper

II. THEORY

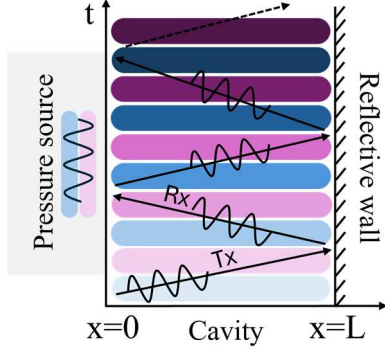


Fig. 2. Illustrations of an acoustic pressure source attached to a cavity of thickness L bounded by an acoustic reflective wall at $x=L$. Multiple transmissions and reflections of ultrasound waves inside the cavity lead to constructive interference and eventually acoustic energy amplification.

Acoustic amplification can be achieved by storing acoustic energy emitted from the ultrasound transducers in an acoustic resonant cavity over time, and releasing it in the form of ultrashort, high-intensity pulses. The resonant cavity is driven by an ultrasound transducer (acoustic resonator). The cavity is initially enclosed by a high acoustically reflective medium. The system can be made analogous to the resonance of a pipe with one end closed and the other driven by a source.

Due to the high acoustic impedance mismatch between the resonant cavity and the reflective medium, the stored acoustic energy undergoes multiple internal reflections inside the cavity (as illustrated in Fig. 1), leading to acoustic energy build-up over time. Once sufficient acoustic energy is stored, the reflective boundary is switched within a very short time to an acoustic transparent medium and the energy is released in the form of a single pulse. This process can be analyzed as follows [9]. Consider a cavity of thickness L , closed at boundary edges $x=L$ [mm] by a reflective wall and at $x=0$ [mm] by a transducer emitting sinusoidal planar acoustic pressure waves (Fig. 2), given by:

$$p(t) = \rho_0 c_0 u_p E(t) \quad (1)$$

where, ρ_0 is the density of the cavity medium, c_0 is the speed of sound in the cavity medium, u_p is the particle velocity in the cavity medium, and $E(t)$ is approximately given by:

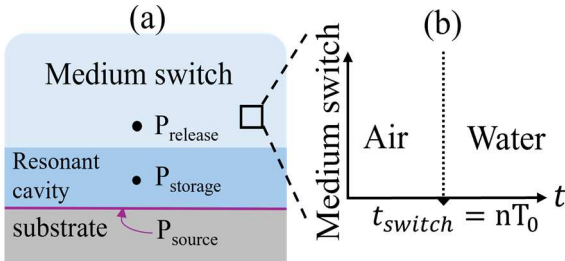


Fig. 3. COMSOL model comprising a substrate, an acoustic pressure source, P_{source} indicated by a line, a resonant cavity where pressure waves are stored and measured within the cavity at a point, P_{storage} and the switchable medium where pressure waves would be released and measured at the point, P_{release} ; (b) Switchable medium consists of medium switching from acoustic reflective (air) to transparent (water).

$$E(t) \sim e^{i(kx - \omega t)} \quad (2)$$

where k is the wave number, x is the position in the acoustic cavity, ω is the angular frequency, and t is the elapsed time. Due to the superposition of the transmitted (Tx) and reflected (Rx) waves from the boundary edges (Fig. 2) we can generalize the superposed waves as (3). On summation, we obtain a geometric series, which is given by (4) for $kL \neq \pi l$.

$$p = \rho_0 c_0 u_p E \left(t - \frac{|x|}{c_0} \right) + \quad (3)$$

$$+ \rho_0 c_0 u_p \sum_{n=1}^{\infty} \left\{ E \left(t - \frac{|x - 2nL|}{c_0} \right) + E \left(t - \frac{|x + 2nL|}{c_0} \right) \right\}$$

$$\frac{p}{\rho_0 c_0 u_p} e^{-i\omega t} = \quad (4)$$

$$= e^{-ikx} \left(\frac{1 - e^{-2ik(N_1+1)L}}{1 - e^{-2ikL}} \right) + e^{ikx-2ikL} \left(\frac{1 - e^{-2ikN_2L}}{1 - e^{-2ikL}} \right)$$

and by (5) for $kL = \pi l$:

$$\frac{p}{\rho_0 c_0 u_p} e^{-i\omega t} = \quad (5)$$

$$= e^{-ikx} (N_1 + 1) + e^{ikx} N_2$$

where N_1 , N_2 and l are given by (6), (7), (8), respectively

$$N_1 = \text{integer} \left(\frac{c_0 t - x}{2L} \right) \quad (6)$$

$$N_2 = \text{integer} \left(\frac{c_0 t + x}{2L} \right) \quad (7)$$

$$l = 1, 2, 3, \dots \quad (8)$$

The resulting expression reduces to (9) for $kL \neq \pi l$,

$$\frac{p}{\rho_0 c_0 u_p} e^{-i\omega t} = -i \cos(kx - kL) / \sin kL \quad (9)$$

and is given by (10) for $kL = \pi l$.

$$\frac{p}{\rho_0 c_0 u_p} e^{-i\omega t} = \cos kx \left(\frac{c_0 t}{L} \right) \quad (10)$$

For $kL \neq \pi l$, and assuming small damping ω (considering small negative imaginary part), p converges towards a finite value, which is the steady state limit, which is given by (9). However, it can be seen from equation (10) that the pressure the resonant frequency as $f_0 = \frac{1}{2}lc_0/L$. It should also be noted that the total acoustic pressure is inversely proportional to the thickness of the cavity L .

III. PROOF-OF-CONCEPT SIMULATION

To observe the effect of acoustic amplification, a finite element model (FEM) of the acoustic stack was developed in COMSOL Multiphysics 6.2 as shown in Fig. 3a. Studies were performed to analyze the effect of acoustic pressure variation with time inside the resonant cavity as well as outside the cavity when the adjacent medium switches from ultrasound-reflective to ultrasound-transmissive.

A. Geometry

A simplified acoustic source, considered as the pressure source, generating planar mechanical waves is given by (11):

$$P_{source} = P_0 \sin(\omega t) \quad (11)$$

The pressure source operates at a resonant frequency (f_0) of 4 MHz. A resonant cavity is placed above the source, which is of Polydimethylsiloxane (PDMS). PDMS is chosen as an example material owing to its low acoustic losses, compatibility with microfabrication processes, and broad accessibility. The cavity thickness is designed as half a wavelength in PDMS ($\lambda_{PDMS}/2 = 132.5 \mu\text{m}$). Adjacent to this resonant cavity is a switchable medium which can be switched at multiple periods of time between two states – a high acoustic impedance mismatch (reflective) and a low acoustic impedance mismatch (transparent). Air, with its large acoustic impedance mismatch relative to PDMS, serves as the reflective medium, while water, with its relatively close impedance match, acts as the transparent medium (Fig. 3b). The medium remains as air when acoustic energy is to be stored within the PDMS cavity for amplification, and switches to water at user-defined integer multiples of the acoustic period (nT_0), also called t_{switch} , to release the amplified energy into the surrounding medium. Here T_0 is the acoustic wave period given by $1/f_0$.

B. Material Properties and Parameters

A non-linear fluid model incorporating general dissipation effects, including sound diffusivity within each material layer, was considered. A Pressure Acoustics, Transient (actd) study was implemented to verify the phenomena of acoustic amplification. For modeling the switchable medium, a step function $step(t)$ was employed, where density and speed of sound in the medium transition from air to water (1 to 0) at a certain integer multiples of the acoustic time period (nT_0).

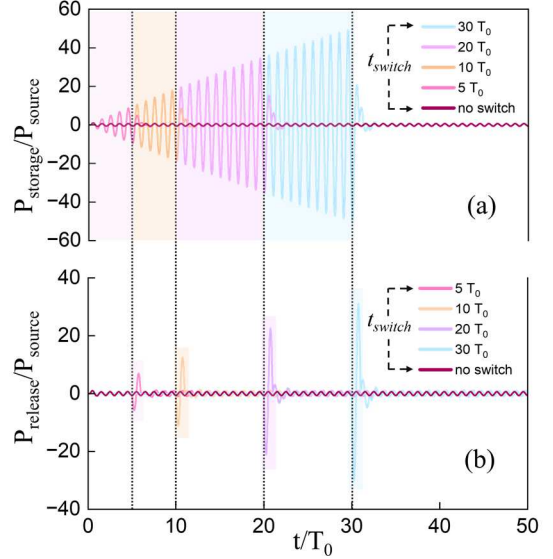


Fig. 4 (a) Acoustic amplification with time inside acoustic resonant cavity when medium switch is air; (b) Released amplified single-pulse of $1 T_0$ ($= 0.25 \mu\text{s}$) wide to the medium.

The medium switch for change in density and speed of sound is given by (12) and (13), respectively:

$$\rho_{water}(1 - step(t)) + \rho_{air}step(t) \quad (12)$$

$$c_{water}(1 - step(t)) + c_{air}step(t) \quad (13)$$

The transition zone was defined with a temporal width of $T_0/50$. A time sweep of range from $t=0$ to $50 T_0$ was performed to observe the effect of acoustic amplification at various t_{switch} . The parameters used for P_0 is of 100 kPa. The material properties of PDMS, water, air and substrate, which is of Silicon (Si), were taken from COMSOL's built-in material library.

C. Results

Fig. 4a shows the pressure stored over time in the PDMS resonant cavity at point $P_{storage}$. The results show that standing waves are established due to the constructive interference

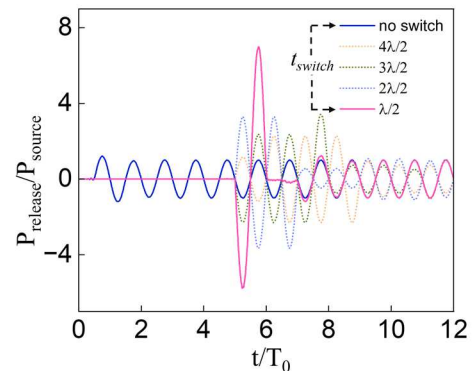


Fig. 5. Acoustic pressure variation with the thickness of resonant-cavity at a certain nT_0 ($=5 T_0$) and when there was no switch, i.e., continuous emission of planar ultrasound waves.

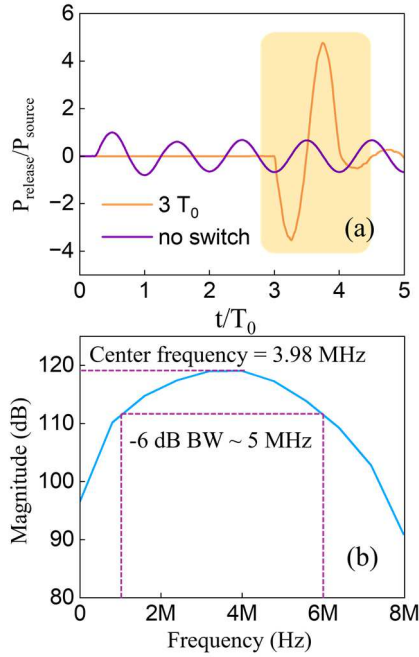


Fig. 6(a) Single-pulse emitted due to acoustic amplification at $t_{switch} = 3 T_0$; (b) FFT of the single-pulse emphasizing on its wide-bandwidth (BW).

between incident waves and reflected waves, as predicted by (10). The ratio of the acoustic pressure at $P_{storage}$ normalized to the pressure at P_{source} ($P_{storage}/P_{source}$), gradually increases over time as long as the adjacent medium is air ($t < t_{switch}$), and this increase is directly proportional to the number of wave-periods in t_{switch} . For reference, the same pressure ratio is shown for the condition when the adjacent medium is always water (no switch), where no pressure increase is observed. Immediately after the adjacent medium is switched to water ($t > t_{switch}$) (Fig. 4b), the stored ultrasound energy is released, and the pressure at $P_{storage}$ highly decreases to a value close to the reference pressure level. On the other hand, after the medium switches to water, the pressure in $P_{release}$ normalized to pressure at P_{source} ($P_{release}/P_{source}$) has the form of a single-pulsed ultrasound wave of approximately one-time period wide, whose pressure magnitude is tens of magnitude higher than the initial input pressure amplitude ($t > t_{switch}$). Thus, each single pulse emitted at t_{switch} increases linearly with t_{switch} , in agreement with (10).

To determine the influence of the resonant cavity thickness on the amplitude of the released pressure wave, the thickness

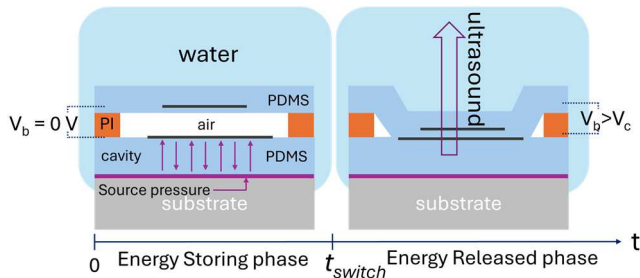


Fig. 7. Illustrations of the MEMS-based shutter for single-pulse high-pressure ultrasound system.

was set to multiples of $\lambda/2$, with the results shown in Fig. 5. These results show that the pressure amplitude of the released pressure wave is inversely proportional to the thickness of the resonant cavity, consistent with (10). It should also be noticed that multiple high-pressure single pulses are emitted when the cavity thickness is increased by multiples of $\lambda/2$.

Fig. 6a further presents the waveform of the single-pulsed, high-pressure ultrasound wave for a particular t_{switch} . To analyze its frequency spectrum, obtained by means of Fast-Fourier transform (FFT), it can be seen that, not only the pressure of the released wave is amplified, but the obtained fractional bandwidth is also high, in this example, 125% (Fig. 6b). This highlights the potential of this approach in ultrasound imaging applications.

IV. FEM OF MEMS-SHUTTER

To realize a fast switchable medium (shutter) in practice, a flexible PDMS-based electrostatic actuator has been envisioned, which can be processed using microfabrication techniques. As shown in Fig. 7, a thin air cavity enclosed by a PDMS membrane supported by a Polyimide (PI) structure or anchor is integrated on top of the PDMS resonant cavity. On applying a bias voltage at t_{switch} across the membrane, the resulting electrostatic force creates a displacement of the suspended PDMS membrane, which is balanced by the mechanical restoring force exerted by the PDMS membrane structure. By controlling the bias voltage (V_b) greater than the collapse voltage, V_c , the membrane starts collapsing onto the PDMS-resonant cavity as the electrostatic force overwhelms the mechanical restoring force (Fig. 7). Once the PDMS membrane fully collapses onto the bottom resonant cavity, the stored acoustic energy in the cavity is released to the adjacent medium. Thus, the acoustic energy storage and release can be controlled electrically through the PDMS-electrostatic actuator, allowing user-defined operation.

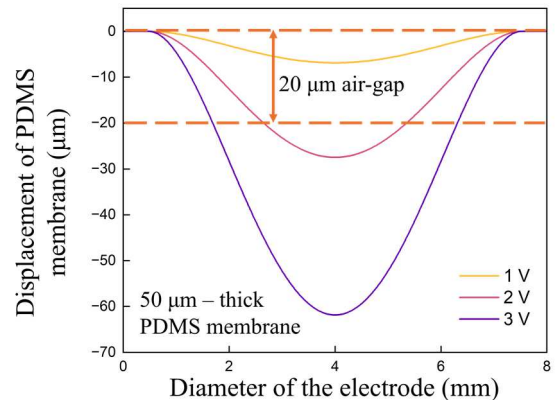


Fig. 8. FEM of the displacement of the suspended PDMS membrane clamped at the edges with polyimide anchors for an electrode diameter of the PDMS membrane and a fixed air-gap.

Fig. 8 shows the FEM of a PDMS-based electrostatic actuator that has a large diameter of 8 mm and a thickness of 50 μm ,

which is separated from the resonant cavity by a very thin layer of air (20 μm), the collapse voltage decreases significantly, for instance, to below 5 V. Such low-voltage operation may enable the entire device to be powered by a battery while maintaining its compact form factor compared to the bulkiness of commercial transducers.

V. CONCLUSION

This work introduced a MEMS-based concept for generating single, high-pressure ultrasound pulses through acoustic energy storage and release. Finite element simulations confirmed that resonant cavities can accumulate acoustic energy and release it on demand as amplified, wide-band pulses. The released waveforms exhibit high peak pressures and broad fractional bandwidths, highlighting potential for both neuromodulation and imaging. Theoretical analysis demonstrated that amplification scales with storage time and inversely with cavity thickness, consistent with the FEM results. A proof-of-concept MEMS-shutter design for the medium-switch based on a PDMS electrostatic actuator was also proposed. Simulations suggest collapse voltages are below 5 V, paving the way for battery-powered operation. Together, these results point to a promising route toward compact, energy-efficient ultrasound systems capable of meeting the demands of next-generation biomedical applications. Future work will focus on microfabrication and experimental validation of the proposed design.

VI. REFERENCES

- [1] R. Beisteiner *et al.*, “Transcranial Pulse Stimulation with Ultrasound in Alzheimer’s Disease—A New Navigated Focal Brain Therapy,” *Advanced Science*, vol. 7, no. 3, Feb. 2020, doi: 10.1002/advs.201902583.
- [2] J. W. Hunt, M. Arditì, and F. S. Foster, “Ultrasound Transducers for Pulse-Echo Medical Imaging,” 1983.
- [3] C. Seok, O. J. Adelegan, A. O. Biliroglu, F. Y. Yamaner, and O. Oralkan, “A Wearable Ultrasonic Neurostimulator - Part II: A 2D CMUT Phased Array System with a Flip-Chip Bonded ASIC,” *IEEE Trans Biomed Circuits Syst*, vol. 15, no. 4, pp. 705–718, Aug. 2021, doi: 10.1109/TBCAS.2021.3105064.
- [4] T. Costa, C. Shi, K. Tien, J. Elloian, F. A. Cardoso, and K. L. Shepard, “An Integrated 2D Ultrasound Phased Array Transmitter in CMOS with Pixel Pitch-Matched Beamforming,” *IEEE Trans Biomed Circuits Syst*, vol. 15, no. 4, pp. 731–742, Aug. 2021, doi: 10.1109/TBCAS.2021.3096722.
- [5] X. Ye, X. Jiang, S. Wang, and J. Chen, “A Low-Intensity Pulsed Ultrasound Interface ASIC for Wearable Medical Therapeutic Device Applications,” *Electronics (Switzerland)*, vol. 13, no. 6, Mar. 2024, doi: 10.3390/electronics13061154.
- [6] E. Moisélo, L. Novaresi, E. Sarkar, P. Malcovati, T. L. Costa, and E. Bonizzoni, “PMUT and CMUT Devices for Biomedical Applications: A Review,” *IEEE Access*, vol. 12, pp. 18640–18657, 2024, doi: 10.1109/ACCESS.2024.3359906.
- [7] K. Roy, J. E. Y. Lee, and C. Lee, “Thin-film PMUTs: a review of over 40 years of research,” Dec. 01, 2023, *Springer Nature*. doi: 10.1038/s41378-023-00555-7.
- [8] Y. Hashimoto and Y. Monnai, “Airborne ultrasound pulse amplification based on acoustic resonance switching,” *Sci Rep*, vol. 12, no. 1, Dec. 2022, doi: 10.1038/s41598-022-23277-8.
- [9] S. W. Rienstra and A. Hirschberg, “An Introduction to Acoustics,” 2021.

